

# Best practices in post-flood surveys: The study case of Pioverna torrent

Alessio Cislaghi,<sup>1,2</sup> Gian Battista Bischetti<sup>1,2</sup>

<sup>1</sup>Department of Agricultural and Environmental Sciences (DiSAA), University of Milan, Milan; <sup>2</sup>Centre of Applied Studies for the Sustainable Management and Protection of Mountain Areas (Ge.S.Di.Mont), University of Milan, Edolo (BS), Italy

## Abstract

Floods cause fatalities and considerable economic damage to infrastructures and settlements, besides impacting fluvial-geomorphic landforms. The increase in the frequency and magnitude of flood events has contributed to inevitably gaining public concern over the flood risk and awareness of the necessity to improve forecasting and monitoring streamflows. In this context, an efficient and systematic procedure of post-event surveys that documents the impacts of a flood event over the territory is often missing. Flood areas delimitation, erosion-sediment variation, and riparian vegetation change are often neglected. The present study shows the field- and desk-based post-flood surveys conducted after an extreme event occurred on June 12<sup>th</sup>, 2019, along the Pioverna torrent in Valsassina (North Italy). The post-flood surveys consist in collecting meteorological data and time-series satellite images to

detect the land cover change (identifying areas covered by water, sediments, and vegetation), and in planning, a few weeks later, an unmanned aerial vehicle (UAV)-based survey to observe the riverbed and streambank change and the modifications in vegetation patterns through high-resolution derived-topographic data. The results show accurate maps of a ground classification from satellite-based elaboration and high-resolution digital elevation models from UAV-based surveys that can support restoration activities and the design of effective countermeasures. This practical application is appropriate and suitable as a river management strategy regarding timing, resources, and economic costs. Thus, standardising the procedure could be essential for creating a historical database, useful to improve specific guidelines and post-emergency management strategies.

## Introduction

Flooding represents one of the most significant natural disasters and is responsible for fatalities and substantial economic damages to buildings and infrastructures (Paprotny *et al.*, 2018). Such dangerous events cause markable changes in fluvial-geomorphic landforms and riparian plant community dynamics, playing a pivotal role in fluvial ecology at the riverscape scale. Geomorphological changes are investigated, especially over medium to long temporal scales (Hooke, 2008; Scorpio *et al.*, 2018) or after large floods (Chappell *et al.*, 2003). Post-event surveys play a crucial role in the post-flood phase gaining experience and knowledge for detecting frequent localised problems (bank erosion, streambank failure, sediments deposition, uprooting of riparian vegetation, *etc.*) and for adapting traditional solutions or exploring alternative countermeasures (*e.g.*, soil and water bio-engineering techniques). Nevertheless, collecting post-flood information is not a simple procedure due to different data precision or aggregation levels.

Moreover, the lack of systematic and comprehensive post-event surveys over the watercourse remains an evident gap in flood risk management and modelling (Borga *et al.*, 2008). Despite the technological advances in fluvial geomorphology and the development of shared operating procedures (Molinari *et al.*, 2017; Taylor and Simeone, 2021), complete and effective documentation of a flood event remains a challenge for fluvial geomorphologists, river engineers, and managers that have to face lack or scarcity of rainfall, streamflow and terrain data (Gaume and Borga, 2008; Marchi *et al.*, 2010; Borga *et al.*, 2011). The unique source of information is the historical orthophotos that provide vegetation and channel patterns at a large temporal and spatial scale. However, accurate data covering pre- and post-flood conditions are usually missing, making the development of reliable hydrological, hydraulic, and hydro-geomorphic models complicated (Tamminga *et al.*, 2015a). For these reasons, geomorpholog-

Correspondence: Alessio Cislaghi, Department of Agricultural and Environmental Sciences (DiSAA), Università degli Studi di Milano, via Celoria 2, 20133, Milan, Italy.

Tel.: +39.02.503.16903 - Fax: +39.02.503.16911.

E-mail: alessio.cislaghi@unimi.it

Key words: Geomorphological changes; remote sensing; post-flood survey; unmanned aerial vehicle; flood.

Acknowledgements: this research was granted by the Territory and Civil Protection Directorate of Lombardy Region (Italy) and the Department of Agricultural and Environmental Sciences of the University of Milan (for the preparation of a river management programme). The authors wish to thank Fernando Altobello (AiPO), Marco Fontana, Alessio Moscaritoli, Angela Nadia Sulis, Diego Terruzzi (Lombardy Region), Paolo Fogliata, Luca Giupponi, Paolo Sala and Emanuele Morlotti (University of Milan) for supporting the field activities.

Received for publication: 23 November 2021.

Accepted for publication: 23 February 2022.

© Copyright: the Author(s), 2022

Licencee PAGEPress, Italy

Journal of Agricultural Engineering 2022; LIII:1312

doi:10.4081/jae.2022.1312

This article is distributed under the terms of the Creative Commons Attribution Noncommercial License (by-nc 4.0) which permits any non-commercial use, distribution, and reproduction in any medium, provided the original author(s) and source are credited.

Publisher's note: All claims expressed in this article are solely those of the authors and do not necessarily represent those of their affiliated organizations, or those of the publisher, the editors and the reviewers. Any product that may be evaluated in this article or claim that may be made by its manufacturer is not guaranteed or endorsed by the publisher.

ical surveys must be carried out immediately after the flood event to identify high-water marks, flooded areas, and sediment supply, especially in gravel-bed rivers. More time passes, and more such signs can be cleaned up by restoration activities or further flood events (Borga *et al.*, 2008).

In this context, with its recent advances, remote sensing is essential to address the challenge of fluvial monitoring. Such technology includes a wide range of techniques and sensors to acquire information, such as digital- and video-cameras, ground-penetrating radar, light detection and ranging (LiDAR), thermal, infra-red, hyper-, and multi-spectral sensors mounted on the satellite, airborne or unmanned aerial vehicle (UAV) (Carbonneau and Piégay, 2012; Entwistle *et al.*, 2018; Tomsett and Leyland, 2019).

Delimitation of flooded areas and vegetation patches can be conducted using satellite images (Wang *et al.*, 2002; Chignell *et al.*, 2015; Rahman and Di, 2017). Increasing satellite passes frequency, satellite image resolution, and computational speed of post-processing algorithms allow to map automatic and quasi-real-time flood mapping (Notti *et al.*, 2018). Despite this, satellite-derived products can be affected by uncertainties and by a lack of accurate validation (Lakshmi, 2017). Meantime, UAV-based surveys can provide higher-resolution terrain data (up to a few centimetres) and can identify different vegetation patterns and sediment erosion-deposition areas (Fonstad and Marcus, 2010; Perignon *et al.*, 2013; Javernick *et al.*, 2014; Micheletti *et al.*, 2015; Picco *et al.*, 2017). UAV technology with photogrammetric software reached a high degree of maturity, extending its application in a broad spectrum of fields, including agriculture, forestry, and landscape management (Torres-Sánchez *et al.*, 2014; Seier *et al.*, 2017; Hashemi-Beni *et al.*, 2018; Tarolli *et al.*, 2020). In addition, UAV-based surveys guarantee flexibility, accuracy, high-spatial-resolution, and low cost due to a broad market of experienced professionals. Thus, the cost-effective photogrammetric platforms provide rapid deployment of on-demand flood mapping.

Although remote sensing offers many advantages, desk-based analysis cannot replace the role of field-campaign. Therefore, planning and standardising a combination of field- and desk-based activities is necessary to balance the considerable consuming resources (time of the high level of technical expertise) and the accuracy of the flood events observations.

In the present study, the primary purpose is to conduct a remote sensing post-flood survey to detect: i) the geomorphological changes, including streambank erosion, sediment deposition, and the stream evolution; ii) the change in vegetation patterns that strongly influence the fluvial geomorphological processes; and iii) the flood-damaged areas including buildings and roads (helpful in estimating economic losses) and hydraulic structures (helpful in giving priority to the restoration works). In addition, a simple methodology has been proposed to balance time-consuming and accurate topographical data, which can improve the forecast of hydrological and hydraulic models and draw specific guidelines and post-emergency management plans.

## Materials and methods

### Study case

The Pioverna torrent is a gravel-bed torrent flowing from east to west along the Valsassina valley into the Como Lake (Lombardy, North Italy; Figure 1) in the proximity of the municipality of Bellano (Lecco province), where the catchment area is

approximately 157 km<sup>2</sup>. Valsassina is a glacial valley characterised by a U-shaped profile. A few stations monitored the meteorological observations inside the catchment, whereas no hydrometeor is located along the torrent. The nearest meteorological station measured, on average, mean annual precipitation of around 1650 mm with peaks in late spring and autumn.

The study case is a 2-km stretch located among the villages of Cortenova and Primaluna, characterised by multiple channels and delimited by well-vegetated streambanks. The riparian zone is dominated by a high-dense forest (25 trees/100 m<sup>2</sup>) composed of several tree species such as white willow (*Salix alba* L.), field elm (*Ulmus minor* Mill.), common ash (*Fraxinus excelsior* L.), and common alder (*Alnus glutinosa* (L.) Gartn.) and by shrubs such as common dogwood (*Cornus sanguinea* L.), common hawthorn (*Crataegus monogyna* Jacq.), and common hazel (*Corylus avellana* L.). The riparian forest is mature (15-20 ages) with a dense canopy cover (hereafter, 'mature vegetation'). Conversely, the streambanks are covered by a pioneer plant community (hereafter, 'pioneer vegetation') where the invasive alien species dispute the empty space with the native species. Here, the black locust (*Robinia pseudoacacia* L.), the butterfly bush (*Buddleja davidii* Franch.), and the Himalayan balsam (*Impatiens glandulifera* Royle) are the dominant invasive species.

### Flood event

The flood event occurred on June 11<sup>th</sup>-12<sup>th</sup>, 2019, seriously hit several municipalities in Valsassina (North Italy) (Figure 1). The meteorological stations in the proximity of the study area began to measure an increase in rainfall at 20:20 on June 11 (Figure 2A). In particular, the storm was initially concentrated into an area delimited by stations 9105, 2152, 14280, and 19335 and then moved towards the northwest. Conversely, the second rainfall peak was recorded by the stations in proximity of Como Lake (stations 19365 and 10585) and then by stations 9105, 14280, and 19335. The meteorological stations measured a cumulative rainfall in 13 hours, ranging between 41.4 mm (station 8097) and 83.0 mm (station 9105), except for the station 19335, which recorded 209.2 mm (Figure 2B). The corresponding return periods, estimated through the moving-window procedure for detecting the maximum rainfall depth observed for each duration (Norbiato *et al.*, 2007) and then the Depth-Duration-Frequency curve (Folador *et al.*, 2021), were approximately 4 years, except for the observations of station 19335 that registered a 300-years return period events. This fact was in accordance with the losses suffered (yellow dots in Figure 1). In fact, this meteorological event caused a significant production of sediment transport from the right-bank tributaries that overflowed the banks, splitting over everywhere, while the remaining part reached the junctions with the Pioverna torrent.

### Time-series satellite images analysis

Time-series satellite images analysis consists in detecting fluvial dynamics by classifying land cover types and comparing pre- and post-flood images. The satellite images were captured by PlanetScope, a constellation of approximately 130 satellites (able to acquire daily collection imagery of 340 million km<sup>2</sup> day<sup>-1</sup>). PlanetScope images were orthorectified scenes, commonly used for various applications. These products were corrected for surface reflectance and delivered as a split frame with 4 spectral bands (blue, green, red, and near-infrared) with a spatial resolution of 3 m. Table 1 summarises the main characteristics of the PlanetScope acquisition system.

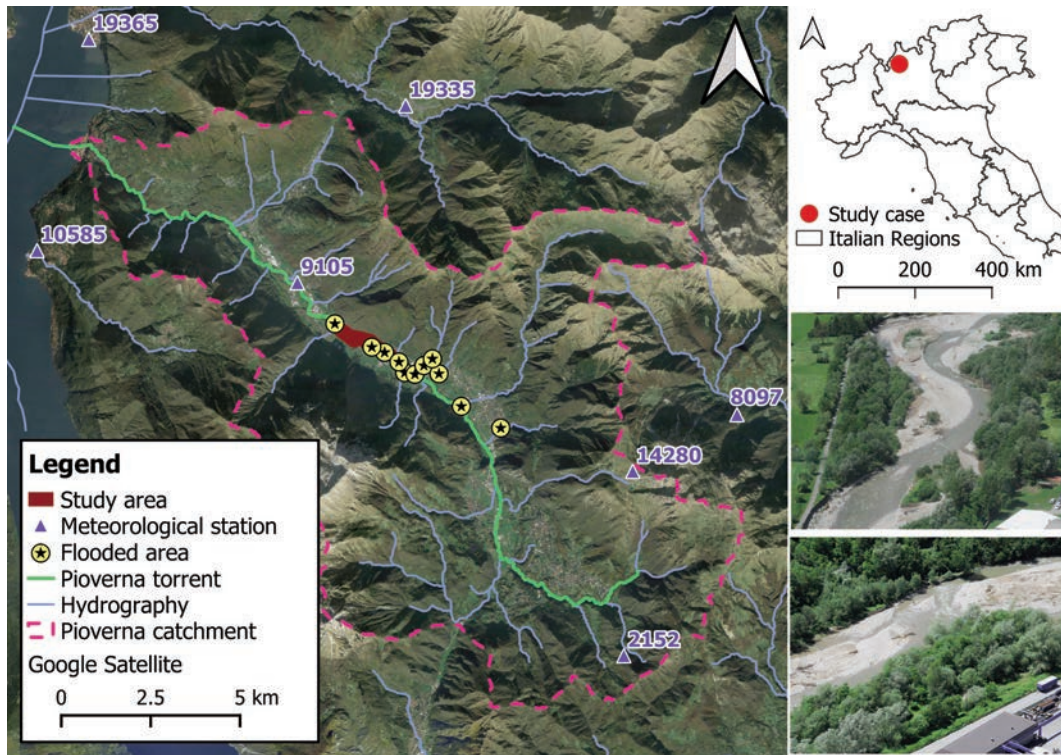


Figure 1. The study domain includes the 2-km surveyed stretch (red line) located along the Pioverna torrent (green line) and 7 meteorological stations (blue triangles). The 11-June flood event caused damage along the main watercourse and the right-bank tributaries (yellow dots).

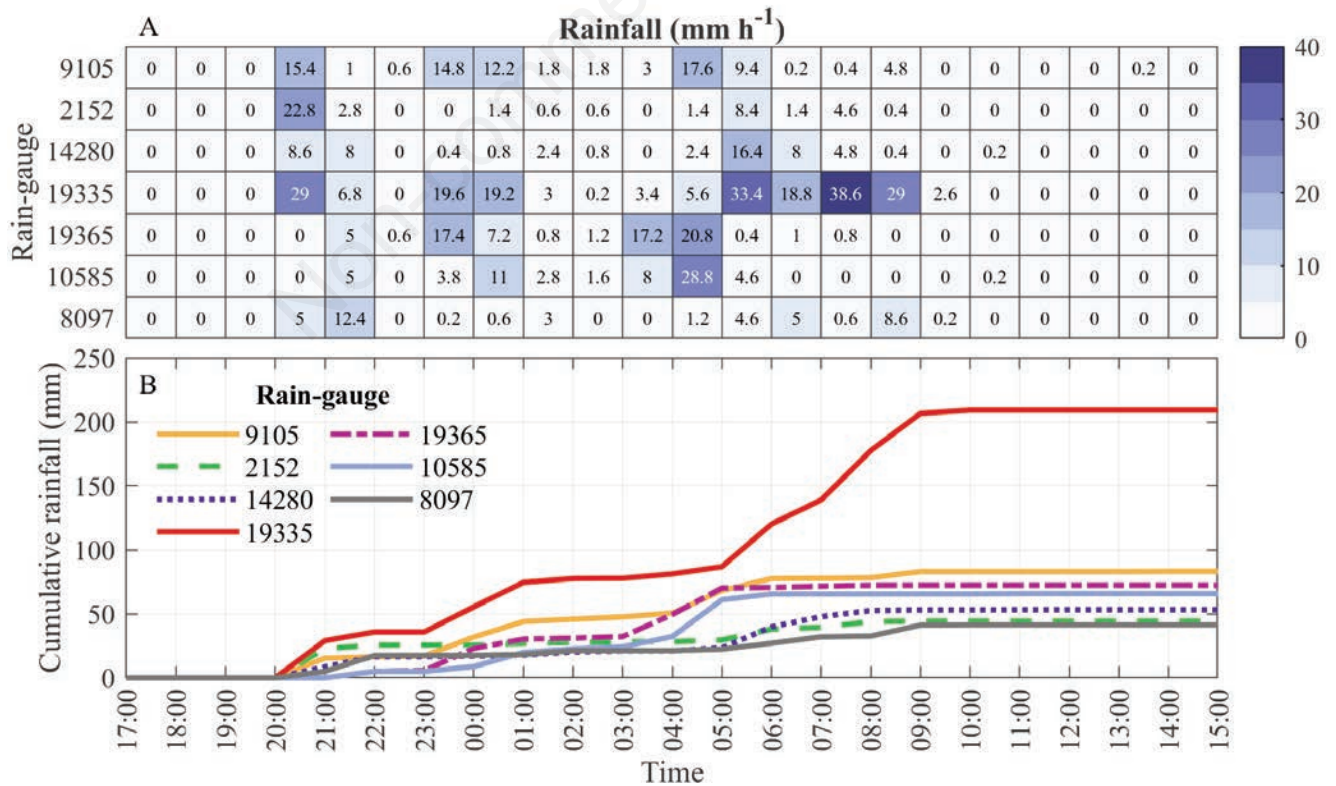


Figure 2. A) Temporal distribution of rainfall intensity ( $\text{mm h}^{-1}$ ) for the 7 meteorological rain-gauges; and B) cumulative precipitation (mm) during the flood event that occurred on June 11<sup>th</sup>-12<sup>th</sup>, 2019.

Then, a supervised pixel classification algorithm was applied to the time-series satellite images to extract the fluvial environment land cover features. This algorithm is the random forests (RF), a non-parametric machine learning technique that combines  $k$ -binary classification and regression trees (Breiman *et al.*, 1984; Breiman, 2001). RF exploits individual decision trees using bootstrap aggregated sampling from 'training areas' (previously classified into desired specific groups, namely, in this case, water, sediments, pioneer, and mature vegetation) with the remaining assigned as out-of-bag samples. A random set of predictor variables is tested at each decision tree node to aggregate sample data into increasing homogeneous subsets. A response variable can be predicted as a categorical classification among all decision trees. Another dataset, the 'test areas,' was used to compute accuracies and error rates averaged over all predictions through the Cohen's Kappa coefficient (Cohen, 1960), a chance-corrected measure of nominal scale agreement among observations and RF predictions.

### Unmanned aerial vehicle-based survey

UAV-system consists of a DJI Mavic 2 Pro Quadcopter equipped with a 20 Megapixel 1' CMOS camera. The drone flight time is approximately 30 minutes for battery charge in the best condition (no wind and no functioning accessories), whereas with the camera attached is about 20 minutes. The camera is characterised by 10-mm lenses (28 mm for 35 mm equivalent) with apertures ranging from f2.8 and f11. The flight plan was designed using Pix4Dcapture, an Android free drone flight planning app (<https://www.pix4d.com/product/pix4dcapture>). The survey covered an area of 0.18 km<sup>2</sup>, which corresponds to a 100 m-wide buffer along the watercourse. Lateral and longitudinal overlaps were set to 60% and 80%, respectively, with a flight altitude between 60 and 70 m. For each survey, 28 ground control points (GCPs) were uniformly spaced along the 2-km stretch at an average distance of 100 m from each other, alternating on the riverbank and the riverbed. The GPCs consist of 0.40×0.40 m bicolour painted wood panels or symbols directly spray-painted onto the concrete. Their coordinates were measured using a real-time kinematic RTK GPS (GRS1, TOPCON) with a vertical precision of 0.02 m. Where possible, the same GCPs were used for the further survey. However, the riverbed modification and the activation of new channel forms prevented all GCPs positions were maintained.

### Structure from motion software and elaboration

Structure from motion (SfM) algorithms has been significantly fostering photogrammetry, improving 3D-models generation by a series of overlapping and convergent digital photographs. Such methodology is now implemented into a broad spectrum of software packages. In the present study, Agisoft Metashape Professional Version 1.5 (Agisoft LLC, St. Petersburg, Russia) was used to elaborate on the images collected by the UAV flight. The software allows to calculate the internal camera orientations and position, align the photographs, and calibrate the parameters related to the characteristics of the camera lenses. The output is a 3D point cloud, 3D mesh, digital surface model (DSM), and orthopho-

tos. In addition, georeferencing procedure improves the quality of the SfM-based outputs minimising the difference with the coordinates of the GCPs.

Furthermore, this software incorporates novel algorithms that perform a dense point cloud classification. This step allows us to identify the ground points automatically and extract the digital elevation model (DEM) directly. The control automatic ground points classification is a machine learning algorithm that depends on the calibration of three parameters: i) max angle (degree) that sets the maximum slope between the points classified as ground; ii) max distance (m) that sets the maximum variation of the ground elevation; and iii) cell size (m<sup>2</sup>) that indicates the maximum size of an area that does not contain any points classified as ground.

### Sediment change assessment

The main output of SfM-elaboration is the difference of DEMs (DoD), obtained cell-by-cell among successive topographic surveys. DoD has been widely exploited in fluvial geomorphology, especially for quantifying the volumetric change along the surveyed stretches. Moreover, producing the DoD is necessary for other purposes, such as: i) inferring bedload sediment transport rate along the surveyed stretch; ii) interpreting processes such as channel scour, fill, migration, and avulsion; iii) mapping the disturbances of ecological habitats; iv) estimating bed levels trends with a certain degree of uncertainty; v) validating complex morphological models; and vi) planning the sediment management over the riverbed for different purposes, from the river restoration to gravel extraction or replenishment schemes (Williams, 2012).

In the UAV-photogrammetry, many factors can introduce errors into the generation of DEM and DoD, such as survey point, survey accuracy, sampling strategy, topographic roughness, and interpolation methods (Lane *et al.*, 1994; Wechsler and Kroll, 2006; Wise, 2007). Assessing the accuracy of generated DEMs from a UAV-based survey could request a comparison with another accurate surface model that is generally not available (Brasington *et al.*, 2003, 2000). Thus, the errors in DEM were estimated by comparing the model elevations with those of GCPs (Lane *et al.*, 2003) and evaluating some performance indices as the mean error (ME), the root mean square error (RMSE), the mean absolute error (MAE), and the standard deviation of error (SDE). Such assessment of DEM accuracy becomes more critical in those geomorphological studies that aim to calculate the sediment budget where the priority step is to calculate the DoD subtracting successive DEMs from each other ( $M.0$  without correction, hereafter). Especially, in this case, propagating the error at spatial scale can help to distinguish false variation in elevation comparing DEMs (Brasington *et al.*, 2003). The simplest method consists in summing the raw volumetric change exclusively upon a critical threshold error  $U_c$  also called Level of Detection (LoD). Such measure of acceptable error can be fixed as the  $D_{84}$  value ( $M.1$ , hereafter; Chappell *et al.*, 2003; Fuller *et al.*, 2003) or calculated as follows ( $M.2$ , hereafter):

$$U_c = t\sqrt{SDE_1^2 + SDE_2^2} \quad (1)$$

**Table 1. PlanetScope bands characteristics.**

Band number	Description	Wavelength ( m )	Resolution ( m )
Band 1	Blue	0.455-0.515	3
Band 2	Green	0.500-0.590	3
Band 3	Red	0.590-0.670	3
Band 4	Near-infrared	0.780-0.860	3

Where the subscripts indicate the two successive raw DEMs assuming a Gaussian distribution of errors, whereas the  $t$  value represents the critical  $t$  values at the selected confidence level. For example, the value of  $t$  can be set at  $t \geq 1$  ( $1\sigma$ ) with a confidence limit of 68% (Lane *et al.*, 2003) or  $t \geq 1.96$  ( $2\sigma$ ) with a confidence limit of 95% (Brasington *et al.*, 2003).

Due to the significant sources of uncertainty, it is largely known that the error is spatially variable and tends to be greater at breaks of the slope where there the local topographic variability is more accentuated as near bars and edges (Heritage *et al.*, 2009). Indeed, considering a uniform error metric across the DEM, the results seem to be over-conservative. Milan *et al.* (2011) proposed a robust procedure to produce a spatially distributed LoD (M.3, hereafter) to solve this problem. The main steps are: i) generating a new standard deviation 0.1-m grid calculated in a 1-m radius-moving window over the two successive raw point clouds. If there are not at least eight data points inside the moving window, a zero value is set to the cell; ii) for each control point and each topographic survey, extracting the standard deviation of elevation error and the difference between modelled and observed elevations, and fitting these variables through a linear regression; iii) the linear regression equations were applied to the standard deviation grids to produce spatial error grids for each survey; and iv) Eq. (1) was applied to obtain spatial error grids and then subtracted from the raw DoD grids.

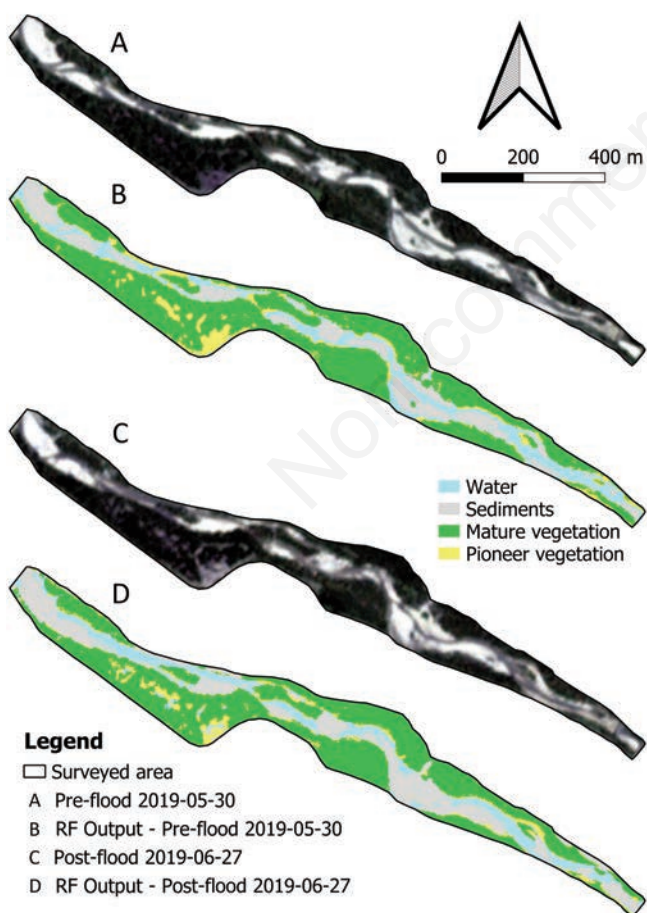


Figure 3. RGB orthophotos surveyed by PlanetScope and RF elaborated imageries of the study area: A) and B) in pre-flood and C) and D) in post-flood condition.

## Results

### Time-series satellite images analysis

Satellite images were captured one time a day. The selection was conducted, excluding all images with more than 25% cloudiness (those acquired during the flood event). For consistency, the pre- and post-flood images were taken on the same days as the UAV-based surveys. Thus, two satellite images were analysed by RF technique for detecting the pre- and post-flood event land cover. The Cohen’s Kappa coefficient was calculated over the RF results over the ‘training areas’ and ‘test areas,’ showing excellent values of performance indices. In ‘training areas,’ the Kappa coefficient was 0.992 and 0.980, whereas in ‘test areas,’ 0.852 and 0.842 for pre- and post-flood images, respectively.

### Riparian vegetation change assessment

Figure 3 provides overviews of the study area’s spatial-temporal distribution of water, sediment, and vegetation. In particular, the vegetation largely covers the flood plain and the streambanks, approximately two-thirds of the entire area. The flood events mainly caused a 5% reduction in the vegetated area and a 7.5% increase in sediment deposits (Figure 4). Bars and channel layout has clearly changed in the middle and downstream part of the study area, significantly reducing the vegetated area. The riparian vegetation particularly covered the left streamside, forming closed canopies that remained unaltered after the flood. Despite the minor differ-

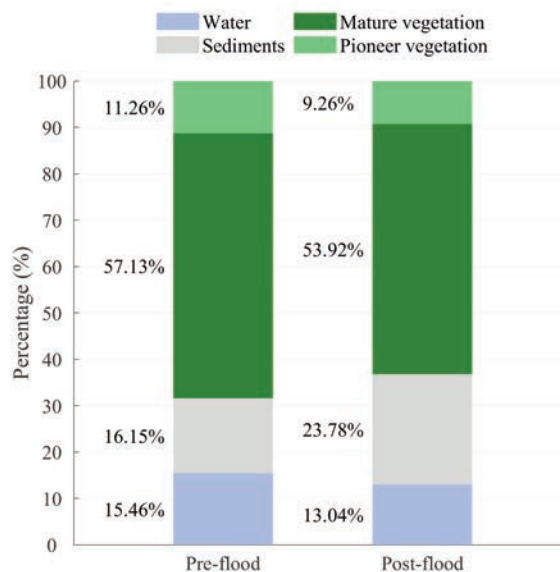


Figure 4. Ground classification through the random forests procedure over two PlanetScope satellite images of the study area. The classification categorises the ground points into water, sediments, pioneer, and mature vegetation.

ence in land coverage ( $-2\%$ ) between pre- and post-flood events, the pioneer vegetation colonised the streambanks, especially in the upstream portion. The vegetated patches, predominantly composed of Himalayan balsam, quickly appeared on the fine sediment deposits in just a few weeks.

### Structure from motion-based output

Two UAV flights were performed pre- and post-flood events to produce detailed DEMs. UAV collected 870 and 703 photos over the study area at the end of each survey. The image processing produced point clouds with a density of 3125 and 2607 points  $m^{-2}$ , respectively. The higher precision of the GCPs guarantees a basis for improving the SfM approach. In fact, using the 28 GCPs as reference points, the photogrammetric algorithms vastly improved the accuracy of the topography generating lower errors, as shown in Table 2. For the planar coordinates of GCPs, the differences are lower than 0.02 m, whereas the elevation errors are at most 0.08 m.

The first products of the SfM procedure are the orthophotos with a resolution of 4.04 and 3.35  $cm\ pixel^{-1}$ , respectively, for pre- and post-survey (Figure 5A and B). Furthermore, DSMs were generated with a high resolution of 2.02 and 1.67  $cm\ pixel^{-1}$ , respectively, and DEMs were extracted, detecting the ground points through the application of the machine learning techniques implemented in the SfM software. Finally, this procedure requests the calibration of three parameters using additional GCPs on the veg-

etated streambanks. In this case, the highest accuracy was obtained by setting the max angle  $10^\circ$ , the max distance 1 m, and the cell size 8 m.

### Sediment change assessment

The spatial distribution of elevation change reveals a complex geomorphological behaviour, characterised by an alternation of erosion and deposition areas, especially in the middle of the surveyed stretch. In detail, in the upstream part, the dominant geomorphological process is the sediment deposition interrupted by significant streambank erosion/failure points. In contrast, in the downstream part, the flood slightly disrupts the sediment balance (Figure 5C). Geomorphic change and sediment transport increased the sediment budget between 2026.72  $m^3$  (M.3) and 2121.94  $m^3$  (M.1). Table 3 shows the sediment change volume in function of the four applied procedures (M.0, M.1, M.2, and M.3; see Section 2.6). The spatial differences in sediment budget change are more evident when analysing several representatives and equidistant cross-sections (Figure 5C). The riverbed showed a marked tendency to deposition along the surveyed area, except for cross-section 3 (Figure 6). In more detail, cross-sections 1 and 2 revealed the most significant volume of deposition ( $+8.26\ m^3\ m^{-1}$  and  $+12.58\ m^3\ m^{-1}$ , respectively), covering more than 70% of the total width. The erosion was concentrated on the right bank in both cross-sections, even if with different intensities ( $-0.43\ m^3\ m^{-1}$  and  $-7.74\ m^3$

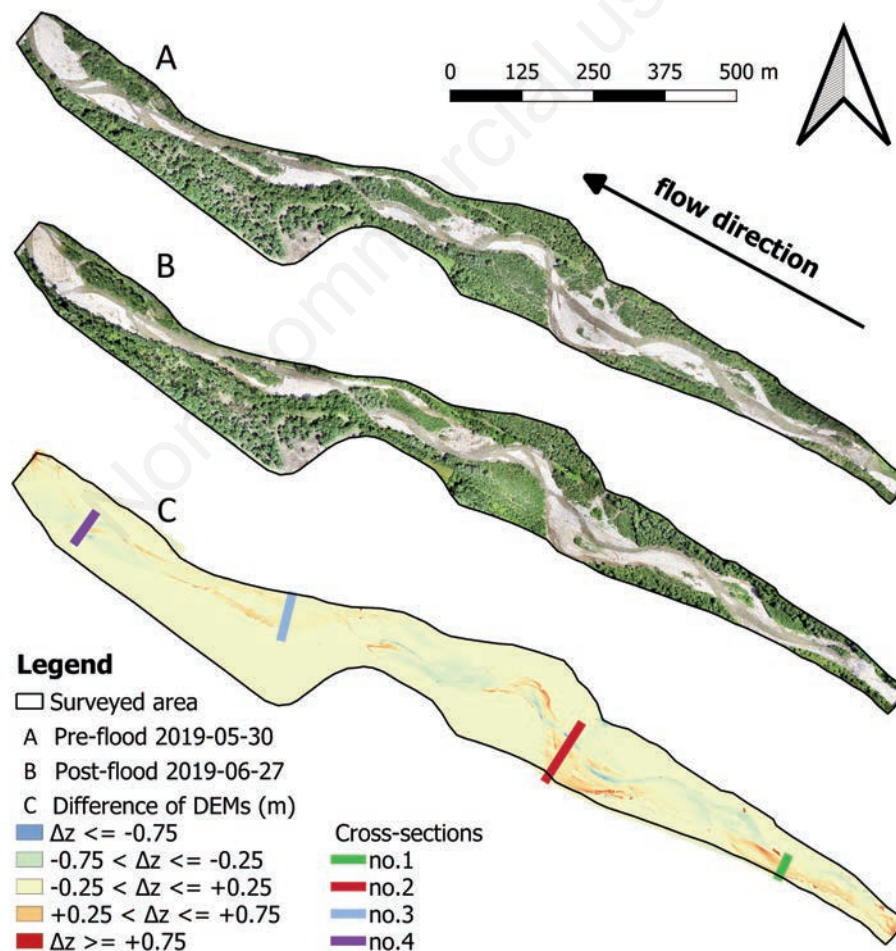


Figure 5. Orthophotos produced by unmanned aerial vehicle (UAV)-based surveys of the study area in A) pre-flood and B) post-flood conditions. The subpanel C) shows the difference between DEMs (DoD) and the positions of the most representative cross-sections.

m<sup>-1</sup>, respectively). Conversely, in cross-section 3, the sediment accumulation was concentrated on the left bank (+2.43 m<sup>3</sup> m<sup>-1</sup>) with a moderate tendency to erosion on the riverbed (-4.61 m<sup>3</sup> m<sup>-1</sup>). Lastly, cross-section 4 showed a significant modification of the transversal shape through the reactivation of secondary channels. In fact, the streambank erosion significantly involved the left bank

of the cross-section (-1.93 m<sup>3</sup> m<sup>-1</sup>), whereas a substantial deposition was evident in the remaining part (+4.14 m<sup>3</sup> m<sup>-1</sup>). The remarkable spatial differences revealed, even more, the high sediment dynamics of the study area exacerbated by the high sediment connectivity from the right-side tributaries and the considerable bed-load sediment transport.

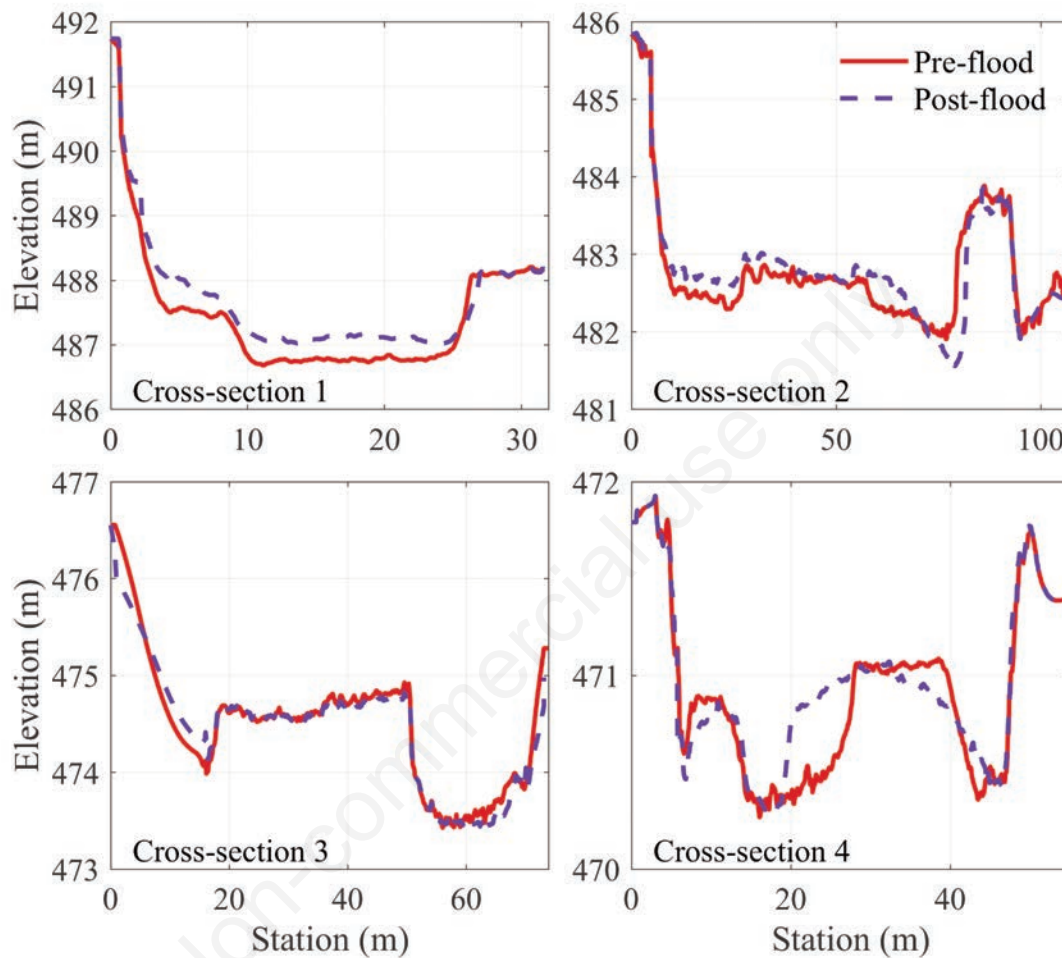


Figure 6. Difference of elevations of 4 representative cross-sections. The red line indicates the pre-flood condition, whereas the blue line the post-flood condition.

Table 2. Digital surface model errors use different performance indices: ME is the mean error, MAE is the mean absolute error, RMSE is the root mean square error, and SDE is the standard deviation error. The subscript 'xy' indicates that the performance index is referred to the planar coordinates, whereas 'z' refers to the elevations.

	ME <sub>xy</sub> (m)	MAE <sub>xy</sub> (m)	RMSE <sub>xy</sub> (m)	SDE <sub>xy</sub> (m)	ME <sub>z</sub> (m)	MAE <sub>z</sub> (m)	RMSE <sub>z</sub> (m)	SDE <sub>z</sub> (m)
Pre-flood	0.002	0.013	0.018	0.017	0.007	0.055	0.078	0.071
Post-flood	-0.001	0.014	0.021	0.018	-0.002	0.041	0.056	0.050

Table 3. Estimating deposition-erosion in the function of different procedures for sediment change assessment.

Procedure	Deposition	Erosion	Balance
M.0	8961.96	-6852.4	2109.56
M.1	7049.39	-4927.45	2121.94
M.2	8627.78	-6534.63	2093.15
M.3	8552.24	-6525.52	2026.72

## Discussion

### Remote sensing for fluvial investigations

Remote sensing technology has been becoming an essential tool for conducting temporal analysis on river processes, consequences of extreme natural events, and natural inheritance to increase the knowledge of conditions, sensitivity, and resilience of the fluvial environment (Gurnell *et al.*, 2016) and for supporting or designing activities of river management and restoration

(Grabowski *et al.*, 2014). Remote sensing includes satellite products and UAV-based surveys now commonly adopted by technicians and researchers.

Image-based elaboration on time-series satellite products allows generating land cover change, detecting areas occupied by water, sediments, pioneer, and mature vegetation and, where possible, the flooded areas. In more detail, the difference among time-series satellite images highlights erosion and deposition of landforms and changes in the vegetated area. These outputs can support the design of requalification and restoration activities and the delineation of the prone-flood zone.

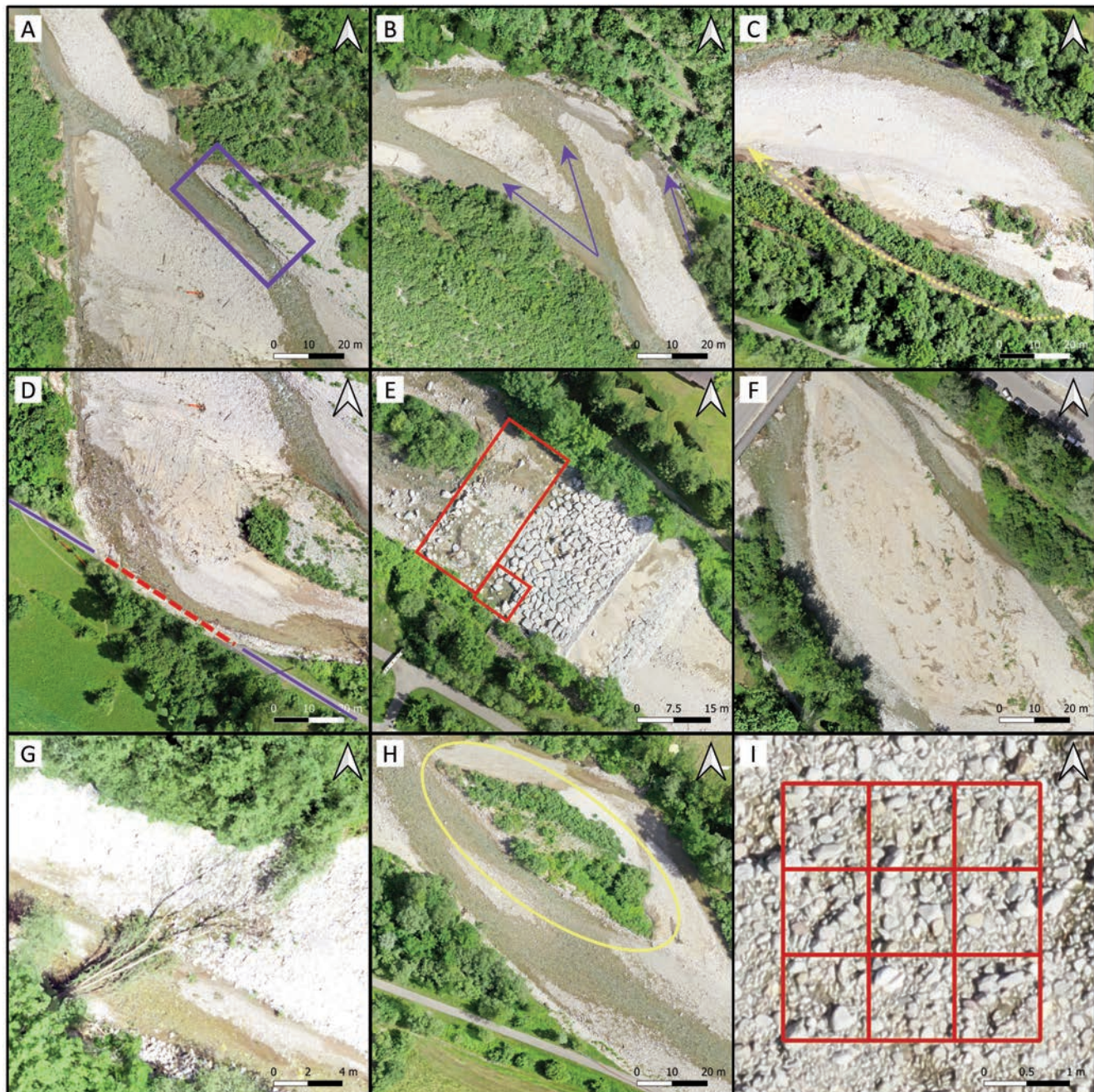


Figure 7. Unmanned aerial vehicle-captured images of A) marked river change, B) activation of secondary channels, C) deposition of fine material along a secondary channel, D) streambank failure causing the cycle path destruction, E) ramp blocks damages, F) in-channel significant wood deposition, G) uprooted tree after the flood, H) spatial distribution of pioneer and mature vegetation over sediment deposition, and I) a vertical photo of 1 m<sup>2</sup> useful for conducting grain size measurements.

UAV-based surveys are a flexible, accurate, and efficient approach for high-resolution topographic monitoring (Tamminga *et al.*, 2015a, 2015b) and for collecting spatial data useful as input for 2D/3D hydraulic modelling. The benefits have increased with recent technological advances, especially feature-based image matching algorithms within SfM software.

Results of SfM elaboration can be of high quality, taking some foresight: i) setting the UAV-equipped camera for acquiring large image overlaps (around 60%-80%) to guarantee highly accurate point clouds (Cucchiari *et al.*, 2018); ii) fixing GPCs along the river on hydraulic structures inside and outside the riverbed as checkpoints (Tamminga *et al.*, 2015a); iii) performing UAV-based survey during low-flow river condition (Lane, 2000); iv) avoiding over predictions of elevations in submerged areas through optical-empirical bathymetric correction or linear relationship between transformed watercolour and water depth (Legleiter *et al.*, 2009); v) reducing errors in DEM where the canopies broadly cover the terrain through a sufficient number of GPCs on the streambank and over the floodplain; and vi) ensuring an adequate area for take-off and landing of the UAV, and for pilot-in-command operating.

In river research and practice, collecting and sharing UAV photogrammetric surveys could be a milestone for river designers and engineers to improve the safety and efficiency of hydraulic interventions, reduce the cost, and plan the operations of river management. The products of UAV-based and remote sensing-based surveys allow detecting several changes in river configuration quickly and accurately:

- *The geomorphological changes* include riverbank erosion, sediment deposition, and the stream evolution of braided channels. In the study case, the flood event activated the whole bed surface up to the lateral levees and generated an essential mobilisation of bed and streambank materials. Figure 7A shows how the hydraulic processes caused a significant bed erosion involving the discharge into the main flow channel with a marked elevation change and increasing the size of the bed armoring layer. Conversely, in other parts of the study case, the flood dynamics simultaneously involved transient secondary channels. For example, Figure 7B shows the marked activation of two secondary channels in the middle and the proximity of the right bank, whereas Figure 7C shows a conspicuous deposition of fine materials along a narrow secondary channel. In general, the tendency to create multi-channel river configuration could be a clear indicator for the river restoration projects: for example, the river managers could design, where there is still enough space, in this case, within the riparian forest, artificial excavated secondary channels to increase the hydrological connectivity, and provide more suitable habitat for other macrophytes, macroinvertebrates, fishes and wading-birds (*e.g.*, Simons *et al.*, 2001).

- *The flood-damaged areas*, including buildings, infrastructures, and hydraulic structures inside the stream, are just useful for estimating economic loss. For example, in this study case, Figure 7D shows the streambank failure that destroyed 85 m-cycle path, whereas Figure 7E reveals the damages of a block ramp, restoring with a dozen of 3 m<sup>3</sup> blocks.

- *The in-channel wood debris* accumulated over the bed surface and against the bridge abutments, including coarse and large woody debris. Figure 7F shows an area of around 235 m<sup>2</sup> covered by dead plant materials and an in-channel large wood volume of around 21.5 m<sup>3</sup> over the pile caps. Figure 7G shows an uprooted tree that fell in the active channel. All these materials, especially those obstructing the space among the piers, must be usually land-filled at an expensive cost.

- *The spatial flow roughness* for 2D and 3D hydraulic modelling includes pioneer vegetation (Figure 7H) and grain size change of sediment bed (Figure 7I). In fact, a UAV-based survey can provide ortho-mosaics composed of 1.5 cm pixel<sup>-1</sup> vertical photo of 1 m<sup>2</sup> useful for conducting grain size measurements of fluvial gravel following robust developed procedures (Carbonneau *et al.*, 2004; Cislighi *et al.*, 2016; Detert *et al.*, 2018), especially determining spatially D<sub>50</sub> and D<sub>84</sub>. Moreover, combining high-resolution orthophotos and DoD can detect the dynamic evolution of riparian vegetation (bare soil, pioneer plant colonisation, and established mature plant community).

### Post-flood survey campaign

This study is part of a field survey campaign conducted to analyse the geomorphological consequences along a 2-km stretch of Pioverna torrent after the flood event on June 12<sup>th</sup>, 2019, in Valsassina (Lombardy, Italy). As outlined in the study of Gaume and Borga (2008), post-event analysis consists in collecting meteorological data and pre-event digital photogrammetric observations, finding field evidence such as high-water marks, detecting evident signs of geomorphologic and vegetation changes, delimiting flood areas and reconstructing peak discharge also through eyewitnesses and local authorities' documents. Rainfall and topographic data can be found immediately after the flood event, whereas the other activities are conducted a few weeks after, at the end of the emergency operations. Meantime, satellite images can be acquired as soon as the cloudiness disappears and can be used to extract the land cover map (and the post-flood differences). Furthermore, a UAV-based survey can be carried out to calculate the geomorphic and elevation change by building the DoD using the permanent GPCs as checkpoints. In addition, phytosociological *relevés* can be conducted on the riparian vegetation communities along several transects of the stream from the riverbank to the active riverbed to detect which are the pioneer species and the ecological succession. Such analysis supports and improves the riverine ecosystem management (Fogliata *et al.*, 2021). Such procedure of post-flood surveys has strategic importance for a broad spectrum of multidisciplinary aspects, from the ecology to the hydraulics, and offers an example of how different tools and activities can be efficiently combined to obtain a faithful reconstruction of the flood event. Moreover, a systematisation and standardisation of post-flood surveys and, as a consequence, their observations, rapidly obtained after the event, can support the design and the choice of specific activities of the post-emergency management that involves the repair of hydraulic structures, the restoration of hydraulic semi-natural fluvial dynamics, the removal of in-channel coarse and large wood if it obstructs the streamflow, and the vegetation control for protecting the native species.

### Conclusions

Watercourses naturally adjust and self-organise the geomorphologic function as a response to all the disturbances (*e.g.*, flood events, riverbed degradation, narrowing, control works), altering sediment and water transfer, exacerbating bank erosion processes and streambank failures, and exposing bare sediment that pioneer species can subsequently colonize. River management has to address fluvial dynamics by planning sustainable practices/technical measures with the aim to combine hydraulic safety, river functionality, and ecological/environmental quality. These actions

require monitoring the geomorphological changes (from the active riverbank to the closer floodplains) over time, especially after extreme flood events. Thus, remote sensing technology that combines machine learning algorithms applied to time-series satellite images and SfM software to UAV-captured photographs offers a viable monitoring approach for decision-making support. In fact, this study clearly showed the evolution/dynamics of vegetated and non-vegetated bars and islands as a consequence of a natural disturbance as a flood event and the quantification of erosion-deposition change along a 2-km stretch of a mountainous torrent. Moreover, the study described a practical application for river managers to identify fluvial dynamics and design appropriate and sustainable countermeasures.

## References

- Borga M., Anagnostou E.N., Blöschl G., Creutin J.D. 2011. Flash flood forecasting, warning and risk management: the HYDRATE project. *Environ. Sci. Policy* 14:834-44.
- Borga M., Gaume E., Creutin J.D., Marchi L. 2008. Surveying flash floods: gauging the ungauged extremes. *Hydrol. Process.* 22:3883-5.
- Brasington J., Langham J., Rumsby B. 2003. Methodological sensitivity of morphometric estimates of coarse fluvial sediment transport. *Geomorphology* 53:299-316.
- Brasington J., Rumsby B.T., Mevey R.A. 2000. Monitoring and modelling morphological change in a braided gravel-bed river using high resolution GPS-based survey. *Earth Surf. Process. Landforms* 25:973-90.
- Breiman L. 2001. Random forests. *Machine Learn.* 45:5-32.
- Breiman L., Friedman J., Stone C.J., Olshen R.A. 1984. *Classification and regression trees*. Taylor & Francis, London, UK.
- Carbonneau, P.E., Lane, S.N., Bergeron, N.E., 2004. Catchment-scale mapping of surface grain size in gravel bed rivers using airborne digital imagery. *Water Resour. Res.* 40:W07202.
- Carbonneau P.E., Piégay H. (Eds.). 2012. *Fluvial remote sensing for science and management*, in: *Fluvial Remote Sensing for Science and Management*. John Wiley & Sons, Ltd, Chichester, UK, pp. i-xx.
- Chappell A., Heritage G.L., Fuller I.C., Large A.R.G., Milan D.J. 2003. Geostatistical analysis of ground-survey elevation data to elucidate spatial and temporal river channel change. *Earth Surf. Process. Landforms* 28:349-70.
- Chignell S., Anderson R., Evangelista P., Laituri M., Merritt D. 2015. Multi-temporal independent component analysis and Landsat 8 for delineating maximum extent of the 2013 Colorado Front Range flood. *Remote Sensing* 7:9822-43.
- Cislaghi A., Chiaradia E.A., Bischetti G.B. 2016. A comparison between different methods for determining grain distribution in coarse channel beds. *Int. J. Sediment Res.* 31:97-109.
- Cohen J. 1960. A coefficient of agreement for nominal scales. *Educ. Psychol. Measure.* 20:37-46.
- Cucchiario S., Cavalli M., Vericat D., Crema S., Llana M., Beinat A., Marchi L., Cazorzi F. 2018. Monitoring topographic changes through 4D-structure-from-motion photogrammetry: application to a debris-flow channel. *Environ Earth Sci* 77:632.
- Detert M., Kadinski L., Weitbrecht V. 2018. On the way to airborne gravelometry based on 3D spatial data derived from images. *Int. J. Sediment Res.* 33:84-92.
- Entwistle N., Heritage G., Milan D. 2018. Recent remote sensing applications for hydro and morphodynamic monitoring and modelling: remote sensing for hydro and morphodynamic monitoring & modelling. *Earth Surf. Process. Landforms* 43:2283-91.
- Fogliata P., Cislaghi A., Sala P., Giupponi L. 2021. An ecological analysis of the riparian vegetation for improving the riverine ecosystem management: the case of Lombardy region (North Italy). *Landscape Ecol. Eng.* 17:375-86.
- Folador L., Cislaghi A., Vacchiano G., Masseroni D. 2021. Integrating remote and in-situ data to assess the hydrological response of a post-fire watershed. *Hydrology* 8:169.
- Fonstad M.A., Marcus W.A. 2010. High resolution, basin extent observations and implications for understanding river form and process. *Earth Surf. Process. Landforms* 35:680-98.
- Fuller I.C., Large A.R.G., Milan D.J. 2003. Quantifying channel development and sediment transfer following chute cutoff in a wandering gravel-bed river. *Geomorphology* 54:307-23.
- Gaume, E., Borga, M., 2008. Post-flood field investigations in upland catchments after major flash floods: proposal of a methodology and illustrations: post-flood field investigations in upland catchments. *J. Flood Risk Manage.* 1:175-89.
- Grabowski R.C., Surian N., Gurnell A.M. 2014. Characterizing geomorphological change to support sustainable river restoration and management. *WIREs Water* 1:483-512.
- Gurnell A.M., Rinaldi M., Belletti B., Bizzzi S., Blamauer B., Braca G., Buijse A.D., Bussetini M., Camenen B., Comiti F., Demarchi L., García de Jalón D., González del Tánago M., Grabowski R.C., Gunn I.D.M., Habersack H., Hendriks D., Henshaw A.J., Klösch M., Lastoria B., Latapie A., Marcinkowski P., Martínez-Fernández V., Mosselman E., Mountford J.O., Nardi L., Okruszko T., O'Hare M.T., Palma M., Percopo C., Surian N., van de Bund W., Weissteiner C., Ziliani L. 2016. A multi-scale hierarchical framework for developing understanding of river behaviour to support river management. *Aquat. Sci.* 78:1-16.
- Hashemi-Beni L., Jones J., Thompson G., Johnson C., Gebrehiwot A. 2018. Challenges and opportunities for UAV-based digital elevation model generation for flood-risk management: a case of Princeville, North Carolina. *Sensors* 18:3843.
- Heritage G.L., Milan D.J., Large A.R.G., Fuller I.C. 2009. Influence of survey strategy and interpolation model on DEM quality. *Geomorphology* 112:334-44.
- Hooke J.M. 2008. Temporal variations in fluvial processes on an active meandering river over a 20-year period. *Geomorphology* 100:3-13.
- Javernick L., Brasington J., Caruso B. 2014. Modeling the topography of shallow braided rivers using Structure-from-Motion photogrammetry. *Geomorphology* 213:166-82.
- Lakshmi V. (Ed.). 2017. *Remote sensing of hydrological extremes*, Springer Remote Sensing/Photogrammetry. Springer International Publishing, Cham, Berlin, Germany.
- Lane S.N. 2000. The measurement of river channel morphology using digital photogrammetry. *Photogram. Record* 16:937-61.
- Lane S.N., Richards K.S., Chandler J.H. 1994. Developments in monitoring and modelling small-scale river bed topography. *Earth Surf. Process. Landforms* 19:349-68.
- Lane S.N., Westaway R.M., Murray Hicks D. 2003. Estimation of erosion and deposition volumes in a large, gravel-bed, braided river using synoptic remote sensing. *Earth Surf. Process. Landforms* 28:249-71.
- Legleiter C.J., Roberts D.A., Lawrence R.L. 2009. Spectrally based remote sensing of river bathymetry. *Earth Surf. Process. Landforms* 34:1039-59.
- Marchi L., Borga M., Preciso E., Gaume E. 2010. Characterisation

- of selected extreme flash floods in Europe and implications for flood risk management. *J. Hydrol.* 394:118-33.
- Micheletti N., Chandler J.H., Lane S.N. 2015. Investigating the geomorphological potential of freely available and accessible structure-from-motion photogrammetry using a smartphone. *Earth Surf. Process. Landforms* 40:473-86.
- Milan D.J., Heritage G.L., Large A.R.G., Fuller I.C. 2011. Filtering spatial error from DEMs: Implications for morphological change estimation. *Geomorphology* 125:160-71.
- Molinari D., Menoni S., Ballio F. (Eds.) 2017. Flood damage survey and assessment: new insights from research and practice. *Geophysical Monograph Series*. John Wiley & Sons, Inc., Hoboken, NJ, USA.
- Norbiato D., Borga M., Sangati M., Zanon F. 2007. Regional frequency analysis of extreme precipitation in the eastern Italian Alps and the August 29, 2003 flash flood. *J. Hydrol.* 345:149-66.
- Notti D., Giordan D., Caló F., Pepe A., Zucca F., Galve J. 2018. Potential and limitations of open satellite data for flood mapping. *Remote Sens.* 10:1673.
- Paprotny D., Sebastian A., Morales-Nápoles O., Jonkman S.N. 2018. Trends in flood losses in Europe over the past 150 years. *Nat Commun* 9:1985.
- Perignon M.C., Tucker G.E., Griffin E.R., Friedman J.M., 2013. Effects of riparian vegetation on topographic change during a large flood event, Rio Puerco, New Mexico, USA: Vegetation effects on topographic change. *J. Geophys. Res. Earth Surf.* 118:1193-209.
- Picco L., Comiti F., Mao L., Tonon A., Lenzi M.A. 2017. Medium and short term riparian vegetation, island and channel evolution in response to human pressure in a regulated gravel bed river (Piave River, Italy). *Catena* 149:760-9.
- Rahman Md.S., Di L. 2017. The state of the art of spaceborne remote sensing in flood management. *Nat Hazards* 85:1223-48.
- Scorpio V., Surian N., Cucato M., Dai Prá E., Zolezzi G., Comiti F. 2018. Channel changes of the Adige River (Eastern Italian Alps) over the last 1000 years and identification of the historical fluvial corridor. *J. Maps* 14:680-91.
- Seier G., Stangl J., Schöttl S., Sulzer W., Sass O. 2017. UAV and TLS for monitoring a creek in an alpine environment, Styria, Austria. *Int. J. Remote Sens.* 38:2903-20.
- Simons J.H.E.J., Bakker C., Schropp M.H.I., Jans L.H., Kok F.R., Grift R.E. 2001. Man-made secondary channels along the River Rhine (The Netherlands); results of post-project monitoring. *Regul. Rivers: Res. Mgmt.* 17:473-91.
- Tamminga A.D., Eaton B.C., Hugenholtz C.H., 2015a. UAS-based remote sensing of fluvial change following an extreme flood event. *Earth Surf. Process. Landforms* 40:1464-76.
- Tamminga A.D., Hugenholtz C.H., Eaton B.C., Lapointe M. 2015b. Hyperspatial remote sensing of channel reach morphology and hydraulic fish habitat using an Unmanned Aerial Vehicle (UAV): a first assessment in the context of river research and management. *River Res. Applic.* 31:379-91.
- Tarolli P., Pijl A., Cucchiario S., Wei W. 2020. Slope instabilities in steep cultivation systems: Process classification and opportunities from remote sensing. *Land Degrad Dev Ldr.* 3798.
- Taylor N.J., Simeone C.E. 2021. Practical field survey operations for flood insurance rate maps, U.S. Geol. Survey Open-File Report 2020-1146.
- Tomsett C., Leyland J. 2019. Remote sensing of river corridors: a review of current trends and future directions. *River Res. Applic.* 35:779-803.
- Torres-Sánchez J., Peña J.M., de Castro A.I., López-Granados F. 2014. Multi-temporal mapping of the vegetation fraction in early-season wheat fields using images from UAV. *Comput. Electron. Agric.* 103:104-13.
- Wang Y., Colby J.D., Mulcahy K.A. 2002. An efficient method for mapping flood extent in a coastal floodplain using Landsat TM and DEM data. *Int. J. Remote Sens.* 23:3681-96.
- Wechsler S.P., Kroll C.N. 2006. Quantifying DEM uncertainty and its effect on topographic parameters. *Photogramm. Eng. Remote Sensing* 72:1081-90.
- Williams R.D. 2012. DEMs of difference. *Geomorphological techniques*. *Br. Soc. Geomorphol.* 2:1-17.
- Wise S.M. 2007. Effect of differing DEM creation methods on the results from a hydrological model. *Comput. Geosci.* 33:1351-65.